Performance, Stability, and Thermal Characterization of a Sub-Kilowatt Hall Thruster

IEPC-2019-910

Presented at the 36th International Electric Propulsion Conference
University of Vienna • Vienna, Austria
September 15-20, 2019

Hani Kamhawi[1], Thomas M. Liu[2], Gabriel F. Benavides[3], Jonathan Mackey[4], Timothy Server-Verhey[5], John Yim[6],
Naia I. Butler-Craig[7]
NASA Glenn Research Center, Cleveland, OH, 44135, USA
and

James Myers[8]
Vantage Partners, LLC

Abstract: This paper describes recent progress at the NASA Glenn Research Center (GRC) in the development and demonstration of an integrated high-propellant-throughput small spacecraft electric propulsion (HT-SSEP) system based on a Hall-effect thruster. A center-mounted cathode and an optimized magnetic circuit topology were implemented in the design of the Hall-effect thruster to achieve high propellant throughput, high performance, and efficient packaging. To minimize technical risk, the HT-SSEP development approach sought to limit design features and materials to those with heritage and a clear path to flight. A propellant throughput capability of greater than 100-kg at a minimum thruster efficiency of 45% was targeted. The proof-of-concept NASA-H64M laboratory model (LM) thruster was designed, fabricated, and tested at GRC in fiscal year 2018. This paper summarizes the motivation for the project, the overall development approach, the chosen sub-system architectures, design considerations, and NASA-H64M LM test results. Detailed information is provided for the performance, stability, and thermal characterization tests of the NASA-H64M-LM thruster. These along with wear characterization tests of the H64M-LM thruster have demonstrated a stable and thermally-viable thruster design with performance levels that exceeded the design objectives. The H64M-LM thruster test campaign demonstrated a thruster that can achieve total thrust efficiency above 48% at a specific impulse > 1,600-sec for a discharge power of 600-W.

I. Introduction

NASA is well-positioned to expand the utilization of lower-cost small spacecraft beyond low earth orbit (LEO) by developing a high-performance and high-propellant-throughput small spacecraft electric propulsion (HT-SSEP) system that leverages NASA advances in Hall-effect thruster technology. By doing so, NASA can advance its strategic

[1] Senior Research Engineer, Electric Propulsion System Branch, Hani.Kamhawi-1@nasa.gov.
[2] Research Engineer, Electric Propulsion System Branch, Thomas.m.Liu@nasa.gov.
[3] Research Engineer, Electric Propulsion System Branch, Gabriel.f.Benavides@nasa.gov.
[4] Research Engineer, Electric Propulsion System Branch, Jonathan.a.Mackey@nasa.gov.
[5] Research Engineer, Electric Propulsion System Branch, Timothy.r.Verhey@nasa.gov.
[6] Research Engineer, Electric Propulsion System Branch, John.t.Yim@nasa.gov.
[7] Student Intern, Electric Propulsion System Branch, Naia.i.Butler-craig@nasa.gov.
[8] Senior Thermal Analyst Engineer, James.l.Myers@nasa.gov.

goal to increase the use of small spacecraft to accomplish its science goals [1]. The lower development and launch costs of smaller spacecraft (< 500 kg) have the potential to increase the cadence of NASA missions and facilitate novel missions requiring numerous spacecraft flying in formations, swarms, or constellations. Before achieving this reality, technical deficiencies with state-of-the-art (SOA) on-board small spacecraft electric propulsion (SSEP) must be overcome including their technology readiness levels (TRL), specific impulses, and/or total propellant throughput capabilities [2].

Electric propulsion (EP) thrusters deliver total impulse magnitudes considerably higher than chemical propulsion systems for a given total propellant mass. This is due to the high specific impulse capability of electric thrusters. The ability to achieve propellant velocities an order of magnitude greater than chemical systems permit solar electric propulsion (SEP) spacecraft to perform similar missions with as little as 10% the propellant mass [3]. Such a massive reduction in propellant mass, compared to a chemical system with comparable propulsive capability, can greatly reduce both the size and launch cost of spacecraft. For these benefits, a growing percentage of large commercial spacecraft are now employing SEP in near-Earth orbits. Similarly, NASA seeks to benefit from advanced SSEP technologies to perform its science goals at lower cost. If SEP can be effectively miniaturized for small spacecraft without significant loss of performance or lifetime, it could usher a paradigm shift through increasing access to space beyond Earth orbits.

An example mission requiring HT-SSEP is a pair of small spacecraft in a 12-hour frozen lunar orbit that can provide near-continuous communication between Earth and rovers or other science instruments located near the lunar poles. Given that transit to these orbits requires a ΔV of 7,100-m/s, a 200-kg spacecraft equipped with a propulsion system with a specific impulse of > 1,685-sec and a duty cycle of 90%, can complete the transit in a year if the thruster efficiency (i.e., ratio of beam power to discharge power) is > 49%. Travel time and minimum thrust efficiency as a function of thrust for a thruster operating at a specific impulse of 1,685-sec is shown in Figure 1 for this sample mission.

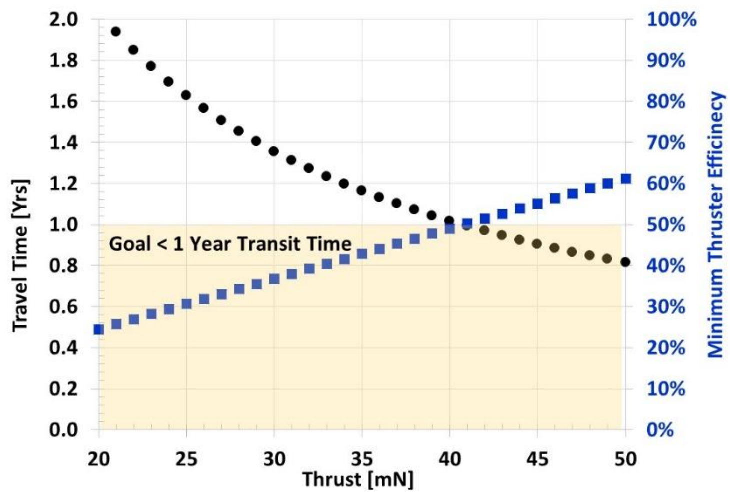

Figure 1. Transit time from 350-km LEO to 12-hr frozen orbit and minimum thrust efficiency for: specific impulse of 1,685-sec, 90% duty cycle, total power of 750-W, and 90% PPU efficiency.

Towards this end, the NASA Space Technology Mission Directorate (STMD) in fiscal year 2018 funded the Sub-Kilowatt Electric Propulsion (SKEP) project through its Game Changing Development (GCD) program. The SKEP project aimed to develop an electric propulsion system (i.e., thruster design, power processing unit design, and feed system concept) at a power, mass, volume, and cost commensurate with the limited resources available to small spacecraft while preserving the substantial performance, propellant throughput, and reliability of SOA higher-power SEP systems. The project leveraged many recent advancements in solar electric propulsion technologies, including from previous NASA investments, and achieved a successful low-power, high-performance HT-SSEP integrated system demonstration (i.e., laboratory-model thruster operated with breadboard discharge power supply). The HT-SSEP system was designed, manufactured, and demonstrated at the NASA Glenn Research Center (GRC) in Cleveland, Ohio. GRC is the lead NASA center for solar electric propulsion and performs in-house SEP technology development activities as well as oversees SEP contracted efforts.

As a consequence of a technology push rather than mission pull, the stakeholders were not well defined in advance of receiving project approval to proceed (ATP). In order to ensure the SKEP team was developing the right technology (i.e., size, power, thrust, interfaces, etc.), an early project task was to identify credible stakeholders willing to provide immediate feedback on the HT-SSEP concept and requirements. The project sought stakeholders internal to NASA as well as feasible end-users from domestic industry. The Planetary Sciences Division (PSD) within the Science Mission Directorate (SMD) proved a key partner in steering HT-SSEP requirements development. GRC also sought input from Goddard Space Flight Center (GSFC) and Ames Research Center (ARC).

From conception, the SKEP project placed equal weight on the HT-SSEP needs expressed by domestic industry as it did NASA stakeholders. While NASA often develops mission-enabling technologies, those technologies are typically transferred to industry at a TRL of 5 (demonstrated laboratory model) for further development and delivery of flight hardware. In theory by doing so, NASA can become a marginal buyer of the technology with future availability of the technology driven by commercial demand rather than ongoing NASA investment. By involving industry early in the development process, the SKEP team sought to balance NASA and commercial needs to better ensure a product with a high likelihood of successful commercialization and future availability to NASA.

Industry feedback was sought through direct project team member participation in conferences and other public technical meetings. Specific attention was given to identifying spacecraft end-users who could provide perspectives based on existing concepts for commercial small spacecraft. The input gathered from credible NASA and industry stakeholders provided the project with the needed direction to define the baseline concept and requirements.

II. Concept of Operations

In order for a HT-SSEP system to be successfully transferred to and commercialized by domestic industry, the unit cost of the HT-SSEP system must be commensurate with the cost of commercial small spacecraft buses. This necessity is a recurring consideration throughout the technology development.

For low-cost small spacecraft, Hall-effect technologies are commonly believed to be the better alternative than gridded-ion thrusters. Hall-effect thrusters are significantly less complex, thus less expensive to develop and fabricate, than gridded-ion thrusters of an equivalent power. The greater complexity of gridded-ion thrusters also translates to greater complexity and cost of the power processing unit (PPU). PPUs are often the most expensive element of an EP system, potentially many times the cost of the thruster. Furthermore, while very high propellant exhaust velocity is desirable for deep space missions, near-Earth missions tend to benefit more from higher thrust. Higher thrust shortens propulsion system operating time and travel time to destinations. For commercial missions, long transit times can result in significant loss of revenues. For national security missions, the ability to transit between orbits or otherwise maneuver rapidly is a tactical benefit. For NASA, the shortened transit time mitigates mission risk due to spacecraft health concerns, such as a decline in solar panel power generation, battery capacity, reliability of electronics, and structural integrity due to micro-meteorite impacts. While both gridded-ion and Hall-effect EP technologies provide NASA with important strategic capabilities, Hall-effect thruster based systems presently appear the stronger demand for small spacecraft electric propulsion due to their performance and lower system cost. For this reason, prior to ATP, the decision was made that the HT-SSEP technology developed under the SKEP project would focus exclusively on a Hall-effect thruster based system.

Accepting that the HT-SSEP technology being developed under the SKEP project is focused exclusively on Hall-effect technology, the concept of operations consistent with stakeholder feedback is as follows. The propulsion system is designed to be capable of:

- generate thrust by electrically ionizing and electrostatically accelerating propellant,
- neutralize the propellant ejected to prevent spacecraft charging,
- include the ability to reverse magnetic field polarity (to switch the direction of the swirl torque),
- protect the spacecraft against all conceivable propulsion system electrical faults,
- include thermal isolation between the thruster and spacecraft to limit spacecraft heating,
- accept an unregulated low-voltage power bus consistent with most small spacecraft,
- accept commands and return telemetry via a common small spacecraft communication protocol,
- require no on-orbit maintenance by the spacecraft other than survival heaters,
- satisfy testing as specified in the NASA GSFC General Environmental Verification Specification (GEVS) when no superseding requirement is recommended [4],
- operate at two qualified firing conditions, including nominal power and a reduced power state,
- operate at additional higher and lower than nominal power firing conditions (although they may not be fully qualified to minimize development cost), and
- employ a scalable, low-cost PPU architecture able to accommodate more than one domestic small spacecraft Hall-effect thruster (since a common PPU minimizes end-user development cost and minimizes mission risk in an environment where it remains unclear which thruster technologies will mature to flight).

Figure 2 is a block diagram depicting the interfaces between a small spacecraft and HT-SSEP device.

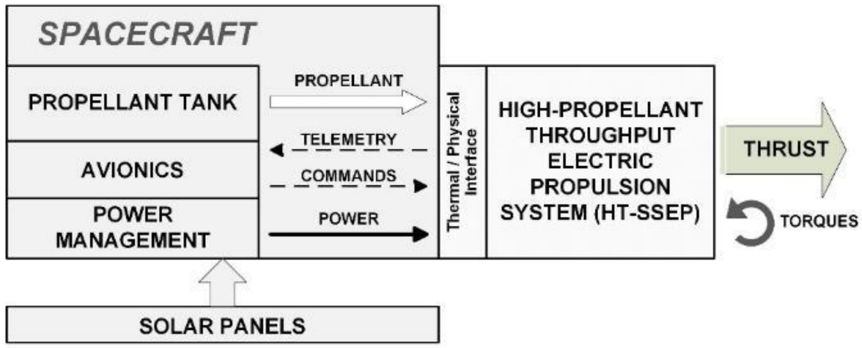

Figure 2. HT-SSEP propulsion system block diagram.

III. Requirements

Thruster, PPU, and propellant feed system requirements were developed and vetted through discussion with stakeholders. For brevity, only select requirements are provided here in Table 1.

Table 1: Select HT-SSEP Requirements

Name	Requirement
Nominal Thrust	The propulsion system shall generate >= 40-mN of thrust at the nominal operating condition over its full operational lifetime.
Nominal Total Specific Impulse	The propulsion system total (anode + cathode flow) specific impulse shall be >= 1600-sec at the nominal operating condition over its full operational lifetime.
Propellant Throughput	The propulsion system shall have a total propellant throughput capability of >= 100-kg at the nominal operating condition.
Propellant	The propulsion system shall meet all performance requirements when fed xenon propellant.
Cyclic Lifetime	The propulsion system shall be capable of 8,000 on/off cycles over its full operational lifetime.
Reversible Swirl Torque	The propulsion system shall have the ability to set the direction of the swirl torque induced by thruster operation.
Input Voltage	The propulsion system shall operate over an input voltage range of 24 to 34-VDC.
Enable Time	The propulsion system shall reach 95% of steady-state thrust in less than 10 seconds following receipt of the enable command.
PMA Outlet Pressure	The propulsion system shall meet all performance requirements when exposed to or operating at a pressure management assembly (PMA) outlet pressures of 40 +/- 3-psia.
System Mass	The propulsion system shall have a mass <= 10-kg (including thruster, PPU, flow controller, and interconnects, but excluding tank, gimbal, and PMA).

IV. NASA-H64M Thruster Development

The thruster architectures considered were limited exclusively to those fitting the classification of Hall effect. An architecture employing a center-mounted cathode was selected for its proven performance and packaging benefits. Electromagnets (rather than permanent magnets) were selected to allow for switching the direction of the magnetic field and in turn the induced swirl torque. This capability reduces the attitude control burden on the host spacecraft. An optimized magnetic field topology that drastically reduces discharge channel erosion was selected to achieve the performance and propellant throughput requirements. A cathode employing a swaged heater was baselined (rather than a heaterless cathode) based on the project's preference towards high-TRL technologies wherever possible to limit development risk as well as to avoid imposing additional complexity on the PPU and feed system architectures.

A. Magnetic Circuit Development

The NASA-H64M thruster's optimized magnetic field topology was designed and simulated in a commercially available magnetics modeling software to provide characteristics found in recent NASA developments necessary to achieve high thruster performance with high-propellant-throughput capability [5] At the same time, the field topology was optimized for a small spacecraft thruster design, which has some differing development challenges from its high-power counterparts. While the initial magnetic circuit simulations were performed using a 2-D model of the thruster to define rough geometries, the final detailed magnetic circuit simulations utilized a full 3-D CAD model consistent with all thruster features as represented in manufacturing drawings.

Extensive and detailed experimental magnetic field mapping of the assembled magnetic circuit was performed. Two dimensional and linear maps were performed at various thruster magnetic current settings. Mapping results showed excellent agreement with magnetic simulation predictions (both 2-D streamline and linear maps along discharge channel centerline). For example, in Figure 3, the thruster's normalized measured channel centerline magnetic field profile at various azimuthal locations proves to be axisymmetric (as predicted by the magnetic simulation). The profile shown in Figure 3 resulted in the desired thruster performance. A short-duration wear test also confirmed the design intent to achieve limited erosion of the discharge channel.

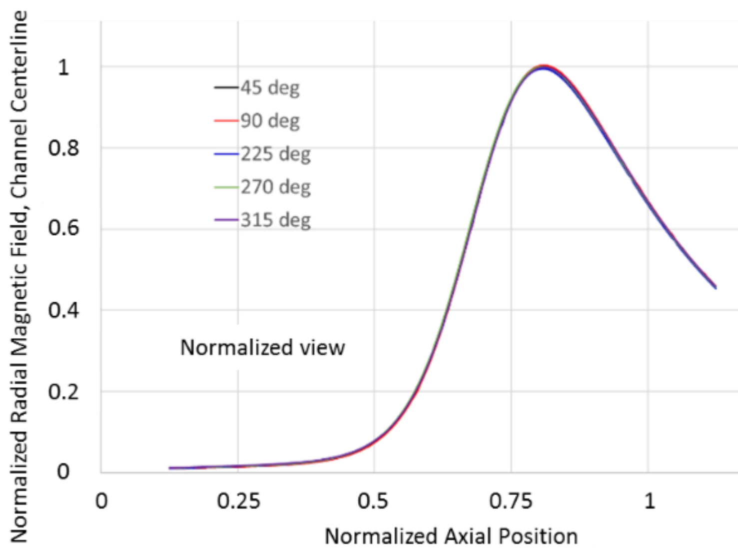

Figure 3. Channel centerline magnetic mapping results at various azimuthal angles for the NASA-H64M-LM thruster.

B. Propellant Distributor Development

Achieving azimuthal neutral flow uniformity in a Hall-effect thruster's channel downstream of the propellant distributor is critical to attaining high thruster efficiencies, minimizing discharge instabilities, and avoiding plume asymmetries [6, 7]. The common approach is integrating the propellant distributor with the discharge anode. A variant of a GRC-heritage design with minor innovations was developed for the NASA-H64M [8] The propellant distributor maintained the key features of the heritage design providing excellent flow uniformity, but made incremental changes to better meet the lower-cost goals for small spacecraft.

Gas flow simulations provided important insight during the anode development. The propellant flow in the upstream portion of the distributor can be effectively described by laminar viscous flow relations and is designed to evenly distribute flow from the inlet around the circumference of the annulus. The effects of flow restrictor variances based on manufacturing tolerances around the anode affect the upstream pressure distribution, and the analysis is iterated to converge on a consistent solution. Monte Carlo procedures were applied to examine the resultant statistical distribution and assess various preliminary manifold designs for their robustness to manufacturing variances and ability to maintain sufficient flow uniformity.

The downstream portion of the distributor, including exit flow into and out of the discharge channel, is in the transitional and rarefied flow regimes and was modeled via a direct simulation Monte Carlo (DSMC) code. Again, multiple preliminary designs and variants were examined to evaluate their ability to provide sufficiently uniform flow that is robust to potential flow and manufacturing variances. Figure 4 illustrates a sample set of discharge channel flow uniformity simulation results that highlight how modest differences in propellant distributor design, including again effects of deviation from various manufacturing tolerances, can lead to substantially differing performance. These gas flow simulations provided important insights informing key propellant distributor design decisions.

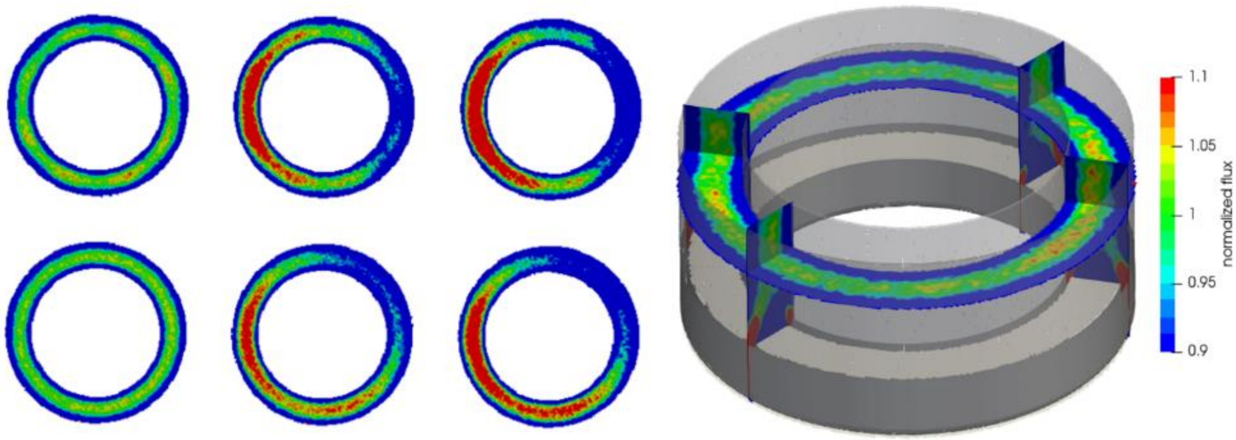

Figure 4. Sample discharge channel flow uniformity simulation results. (Left) 2-D flux distributions for various design implementations. (Right) 3-D flux distribution for a single design implementation.

Following propellant distributor manufacturing, experimental flow characterization was conducted in GRC's Vacuum Facility 8 (VF-8). The distributor was mounted in an aluminum housing geometrically identical to the NASA-H64M-LM's ceramic discharge channel. The facility background pressure was approximately 2-μTorr, while xenon propellant was fed into the propellant distributor's inlet at rates ranging from 10 to 30-sccm. Downstream of the propellant distributor's plasma-facing surface, a pressure transducer mounted on a 4-axis motorized stage made measurements at 11.25° azimuthal angular increments. At each azimuthal angle, nine data points were acquired at the locations as indicated in Figure 5. These locations spanned radially from the inner to the outer channel walls and axially from the mid-channel to the thruster exit plane.

Figure 5 also shows a representative example of the flow uniformity experimental characterization results overlaid on the theoretical prediction. The normalized pressure transducer data for the mid-channel, channel-centerline location is shown for a xenon flow rate of 25-sccm. Both the simulation and test data indicate excellent azimuthal neutral flow uniformity to within ±5%.

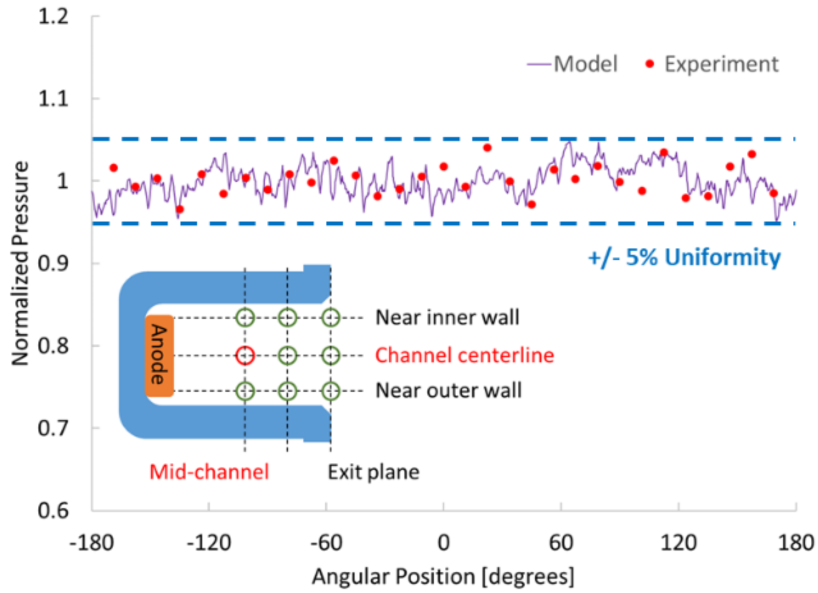

Figure 5. Azimuthal neutral flow uniformity results at the mid-channel, channel-centerline location for the NASA-H64M-LM propellant distributor operating with a 25-sccm xenon flow.

C. Low-Current Hollow Cathode Assembly Development

The NASA-H64M cathode assembly leveraged NASA GRC's long heritage with the development and manufacture of flight hollow cathode assemblies. The present design maintains these heritage design approaches wherever possible, although some allowances were made for the unique packaging requirements [9].

To operate nominally over the range of 1-A to 3-A emission current with an anticipated lifetime in excess of 10,000-hours, the hollow cathode design was scaled from prior designs in order to meet the necessary thermal requirements for efficient plasma production. Building off prior work on small cathodes [10, 11, 12], the cathode was sized to ensure the cathode reached the required temperatures as well as fit within the volume allocation within the H64M thruster. The cathode tube and orifice dimensions were scaled based on lessons from the prior work to ensure the emitter temperature reached the nominal operating temperature of 1050 °C and maintain a sufficiently high internal pressure [13]

Once cathode assemblies were fabricated, they underwent testing in GRC's VF-56 vacuum test facility. This facility is a 0.9-m diameter, 0.9-m long chamber, whose cryopump can achieve a base pressure of ~5 x 10^{-6} Torr. Laboratory power supplies, diagnostics, and data acquisition systems were used throughout all experiments with some exceptions during integrated system testing. These tests determined the appropriate heater operating conditions for cathode conditioning and ignition, demonstrated diode and triode mode operation to the keeper and an external anode respectively, and characterized plume-mode transition behavior. Additionally, cathode temperature measurements were made via thermocouples and optical pyrometry. Figure 7 shows representative data from the first fabricated cathode installed in the H64M indicating discharge voltage as function of emission current and xenon flow rate. The results are in line with expectations based on prior GRC cathode development work.

An alternative approach that exists for power-restricted thruster systems is to use a heaterless hollow cathode. Rather than initiating thermionic electron emission by pre-heating the cathode emitter with a swaged heater, the PPU raises the keeper voltage until a Paschen breakdown occurs. As the cathode self-heats, the emitter transitions to thermionic emission for cathode operation. Heaterless cathodes, in principle, resolve a potential risk by eliminating the need for the swaged heater of heritage devices. While heaterless cathodes have been used in industrial processes where maintenance can be accommodated, they are still considered low TRL for spaceflight application because the approach has not been validated in ground life testing or space use. Additionally, the heaterless cathode startup can place an increased burden on the complexity of the PPU and propellant feed system design [14]. Thus, the operational benefits by implementing a heaterless cathode need to be carefully assessed against other system impacts to complexity and cost. A more tangible advantage of the heaterless cathode is its packaging benefits. For small thrusters, removing the cathode heater provides an attractive relaxation of design limitations for center-mount cathodes. With heaterless cathodes, Hall-effect thrusters with center-mount cathodes can in theory get smaller than exemplified by the NASA-H64M-LM. That said, at the scale of the H64M, a largely heritage cathode with swaged heater has been demonstrated to package acceptably. As such, given the project preference towards heritage technologies for this development, the swaged heater approach was baselined.

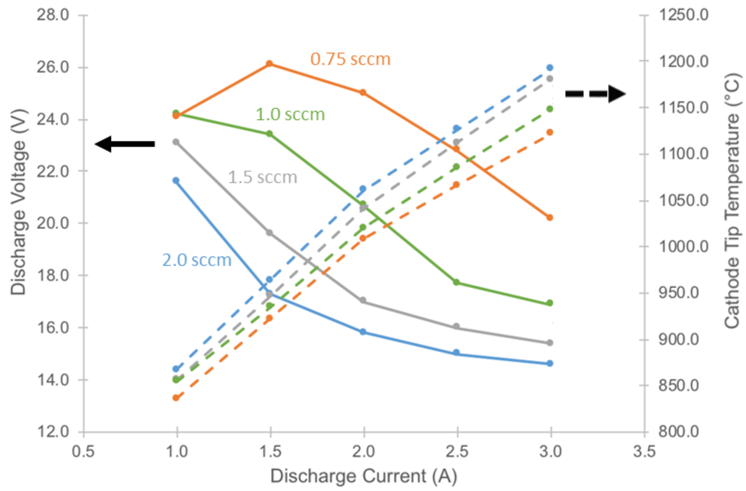

Figure 7. Hollow cathode diode-mode characterization as a function of xenon flow rate.

D. Thruster Thermal Modeling

Typical Hall-effect thrusters, depending on their design power density, see temperature swings from -40°C to 600°C during regular operation on plasma-wetted components, with cathode temperatures exceeding 1000°C. As such, careful thermal design is a key consideration during any thruster development. For electric propulsion systems, heat dissipation on orbit favors passive modes. As such, heat generated by the internal components must be conducted to the exterior surfaces of the thruster for rejection via radiation. Nearly all of these conductive paths can have multiple interfaces that must be designed to efficiently transfer heat, yet mitigate thermal stresses, particularly in the ceramic components.

Development of a detailed thermal model of the thruster assembly correlated to test data is a practical and efficient method to predict the temperatures of all components and thermal impacts of design decisions. For the NASA-H64M-LM, a computational thermal model was developed to ensure that the design has sufficient heat dissipation and that components remain within allowable temperature limits under all operating and environmental conditions. This model, accounting for the entire thruster assembly as well as all conductive and radiative exchange of thermal energy, was developed in a commercially available thermal modeling software by expanding on modeling techniques used on prior NASA GRC Hall-effect thrusters [15]

For the thermal model, resistive heating of the magnetic coil windings were applied based on observed thruster magnet power requirements at steady-state operating conditions. A sub-model of the cathode assembly was constructed to estimate heat loads from the emitter necessary for sustained cathode operation. Plasma heating on thruster surfaces was initially estimated based on prior Hall-effect thruster development data and then subsequently adjusted during model correlation to match H64M-LM thruster measured temperatures.

The resultant model yields steady-state solutions to estimate peak temperatures as well as transient solutions to predict temperature profiles during thruster start-up, operational changes, and cool-down. Figure 8 shows an example result of the NASA-H64M-LM's thermal simulation at the 500-W, 300-V discharge operating condition.

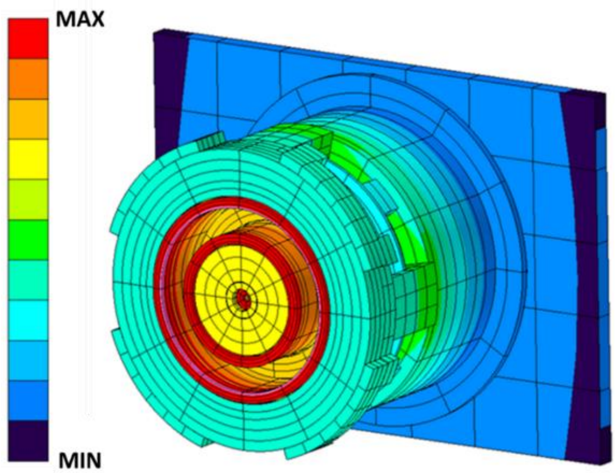

Figure 8. Steady-state thermal model results for NASA-H64M-LM operating at a 500-W, 300-V discharge in which all heat is dissipated to the environment via radiation.

V. NASA-H64M-LM Thruster Test Results

Performance, stability, wear, and thermal characterization was conducted on the NASA-H64M-LM to demonstrate the design's viability for supporting small spacecraft propulsive needs. Vacuum test facilities utilized during the NASA-H64M-LM's development included GRC's VF-8 and VF-56. The VF-8 facility, shown in Figure 9, is a 1.5-m diameter, 4.5-m long chamber whose pumping train (including four 35-inch diameter oil diffusion pumps) can achieve a base pressure of ~4 x 10^{-7}-Torr. A displacement-style, inverted-pendulum thrust stand of heritage GRC design [16] was installed in VF-8 and tuned for low-thrust measurements with a maximum uncertainty [17] of ±2 % of measured value.

Tests of the NASA-H64M-LM (hereafter referred to as H64M) and a version with a 15% wider channel (referred to herein as the H64M-W), were performed in the late summer and early fall of 2018. Table 2 summarizes the major test phases. Over this entire test campaign, the H64M (and H64M-W) thruster accumulated approximately 443 hours of total operating time. The sections below will highlight the major findings from the various test phases. All major test phases are presented in this paper with the exception of Phases B and E; wear results from those phases will be presented as part of a future publication.

Table 2: Summary of major thruster testing phases for the H64M and the H64M-W.

Phase	Thruster	Description	Duration [hr]
A	H64M	Performance and stability characterization: *200 to 600-W discharge power, 200 to 350-V discharge voltage, magnetic and cathode flow fraction mapping*	27
B	H64M	Short duration wear: *500-W, 300-V discharge condition*	275
C	H64M	Performance and stability characterization: *200 to 600-W discharge power, 200-V to 350-V discharge voltage, magnetic and cathode flow fraction mapping*	5
D	H64M	Thermal characterization: *300-W to 600-W discharge power, 300 and 350-V discharge voltage*	18
E	H64M	Accelerated wear characterization: *500-W, 300-V discharge condition*	108
F	H64M-W	Performance and stability characterization: *300-W to 700-W discharge power, 300-V and 350-V discharge voltage, magnetic and cathode flow fraction mapping, integrated demonstration with breadboard discharge module*	10
		Cumulative Thruster Operation	**443 hrs**

Figure 9. GRC's VF-8 test facility utilized for H64M thruster testing.

A. H64M Performance Characterization

Performance and stability characterizations of the H64M thruster were performed in GRC's VF-8 vacuum test facility. Performance was measured at fourteen operating conditions to assess the thruster's throttleability, with discharge powers ranging from 200 to 600 W and discharge voltages ranging from 200 to 350 V. Most testing was performed with the thruster body in an electrically floating configuration, but grounded and cathode-tied electrical configurations were also evaluated for selected operating points. [18,19] At each operating point, magnetic mapping was conducted across a dynamic range of .75 to 1.25 of nominal field setting to assess discharge stability. The cathode flow fraction was also varied from 5 to 11% for selected operating points.

Figure 10 shows an example dataset of results for the thruster at beginning-of-life (BOL) with performance-optimized magnetic field strengths, a cathode flow fraction of 7%, and an electrically floating configuration. These test results were obtained at operational facility pressures of ~7-μTorr-Xe or lower. Uncertainty propagation yields a maximum uncertainty of ±3% and ±5% on specific impulse and thruster efficiency values, respectively. Overall performance values compare favorably against state-of-the-art Hall-effect thrusters in the same power class [20, 21, 22].

Figures 11a and 11b presents the corresponding discharge current ripple data for the thruster's operating conditions presented in Fig. 10. From results presented in Figure 11a, it is observed that the discharge current peak-to-peak (p2p) gets lower as the thruster is operated at a higher discharge current, a similar trend is observed in Fig. 11b with the discharge current RMS. This indicates that for the sizing of the H64M, operation at the design current density provides for efficient and more stable performance. For example, at a discharge voltage of 300-V, Fig. 11a indicates that the thruster discharge current waveform p2p decreases from 200% to 30% as the thruster's discharge current increases from 0.67-A to 2-A.

Cathode flow fraction (CFF) studies were performed at two thruster operating conditions of 1-A and 1.67-A at a discharge voltage of 300-V (300-W and 500-W). For both operating conditions, the CFF was varied between 5 and 11% in increments of 2%. For thruster operation at 300-W, the cathode-to-ground voltage varied from -15.5 to -14.6-V and the thrust varied from 19.4-mN to 19.5-mN. For thruster operation at 500-W, the cathode-to-ground voltage varied from -13.0 to -11.1-V and the thrust varied from 34.4-mN to 34.5-mN as the CFF was varied between 5 and 11%. As such, these results indicate that changing the CFF had minimal impact on the thruster operational performance.

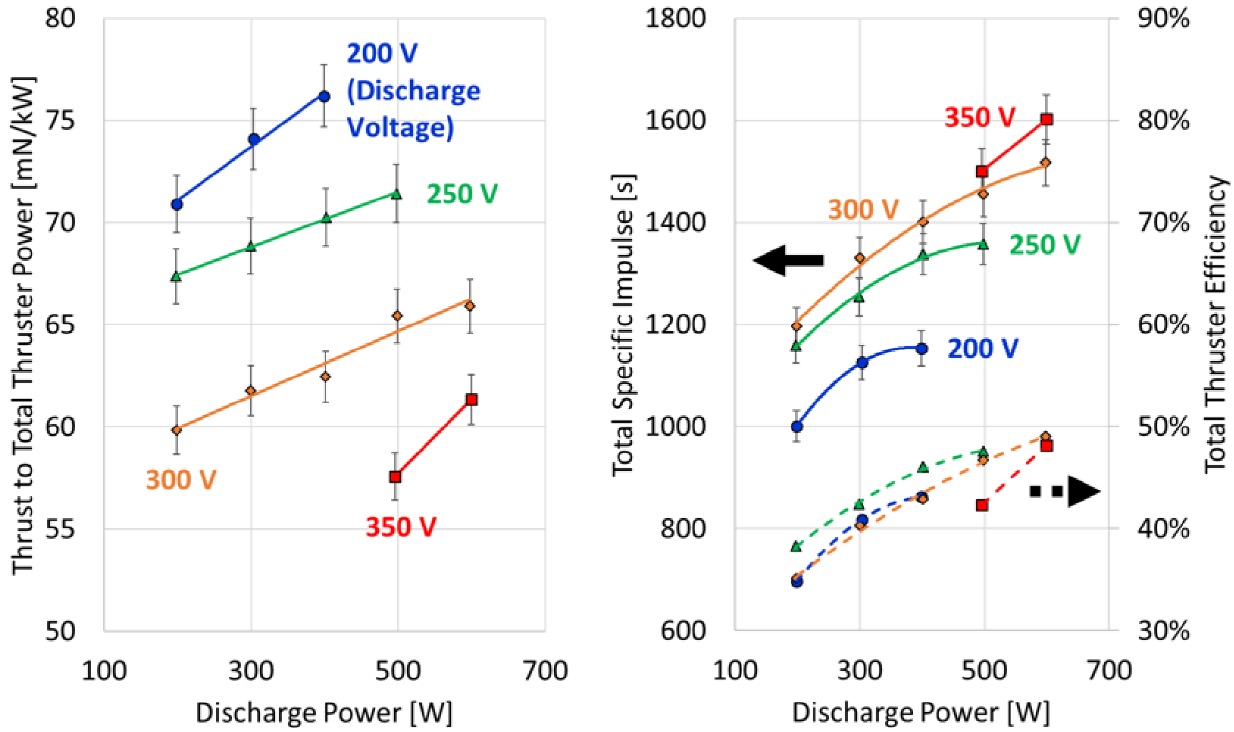

Figure 10. H64M performance at beginning-of-life (BOL) with performance-optimized magnetic field strengths, 7% cathode flow fraction, and electrically floating configuration. The total thruster efficiency uncertainty bars (up to a maximum of ±5%) are not shown for clarity.

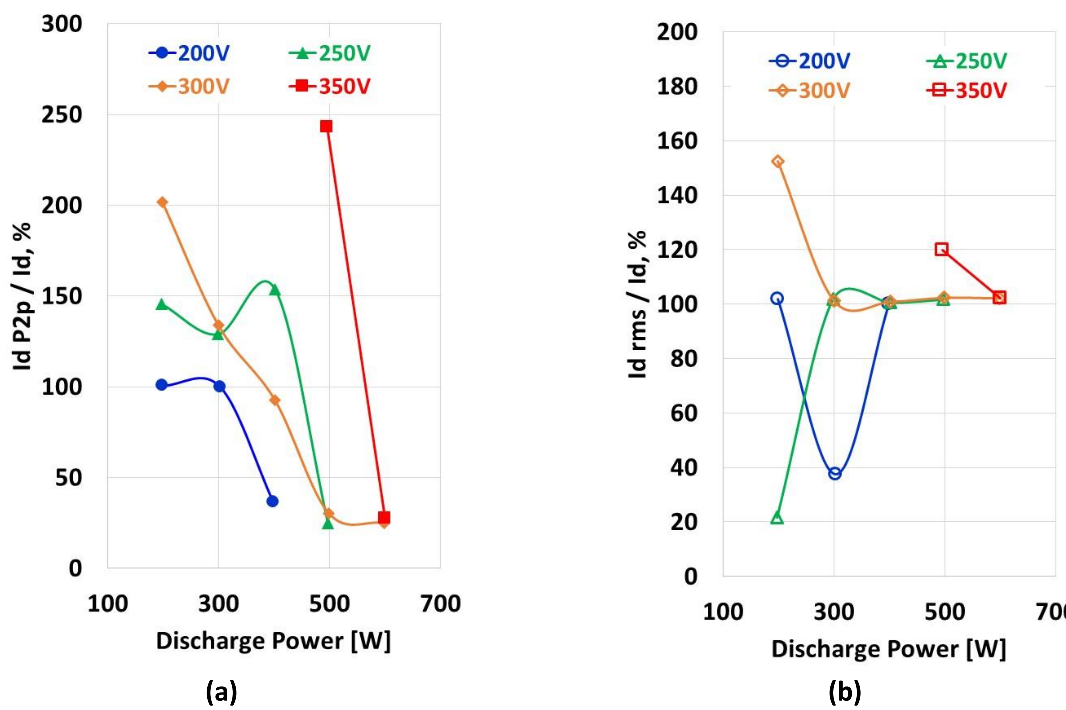

Figure 11. H64M discharge current ripple at beginning-of-life (BOL) with performance-optimized magnetic field strengths, 7% cathode flow fraction, and electrically floating configuration.

B. H64M Short Duration Wear

Following BOL characterization (Segment A) of the H64M, the thruster was operated at the 500-W, 300-V discharge condition (1.67-A discharge current) for approximately 275-hours. The thruster's magnetic field was fixed to a set point that provided optimized thruster performance. During the wear test, the thruster's anode flow was manually adjusted to maintain the thruster's discharge current at approximately 1.67-A. All thruster telemetry was recorded by a data logger with the exception of current waveforms, which were manually recorded and analyzed. The data logger was interlocked with the thruster's power rack, allowing for automatic test shutdown if thruster telemetry alarm conditions were met. Wear testing of the thruster was initiated on August 1, and the test was ended after achieving 275 hours on August 13.

Figure 12a presents a time history of the thruster's discharge current, anode flow rate, and thrust during the 275-hours of operation. Plots in Fig. 12a show that during the test, the thruster flow rate was adjusted slightly (increased from 22.37 to 22.87-sccm) to maintain the discharge current at 1.67-A. No corrections to the thrust magnitude were made during this wear test because the main objective for the test was to accumulate hours on the thruster and detailed performance mapping was planned at the conclusion of the test. Figure 12b shows the corresponding discharge current ripple profiles during the short wear test. Fig. 12b indicates that the thruster's discharge current p2p started around 20% and increased to approximately 40% by hour 275. In addition, the thruster's discharge current RMS varied throughout the test; this suggests that the thruster oscillatory behavior varied during the test due (most likely) to slight erosion of the discharge channel. Changes is thruster performance and discharge current ripple characteristics has been observed before in other Hall thruster of similar power [23]

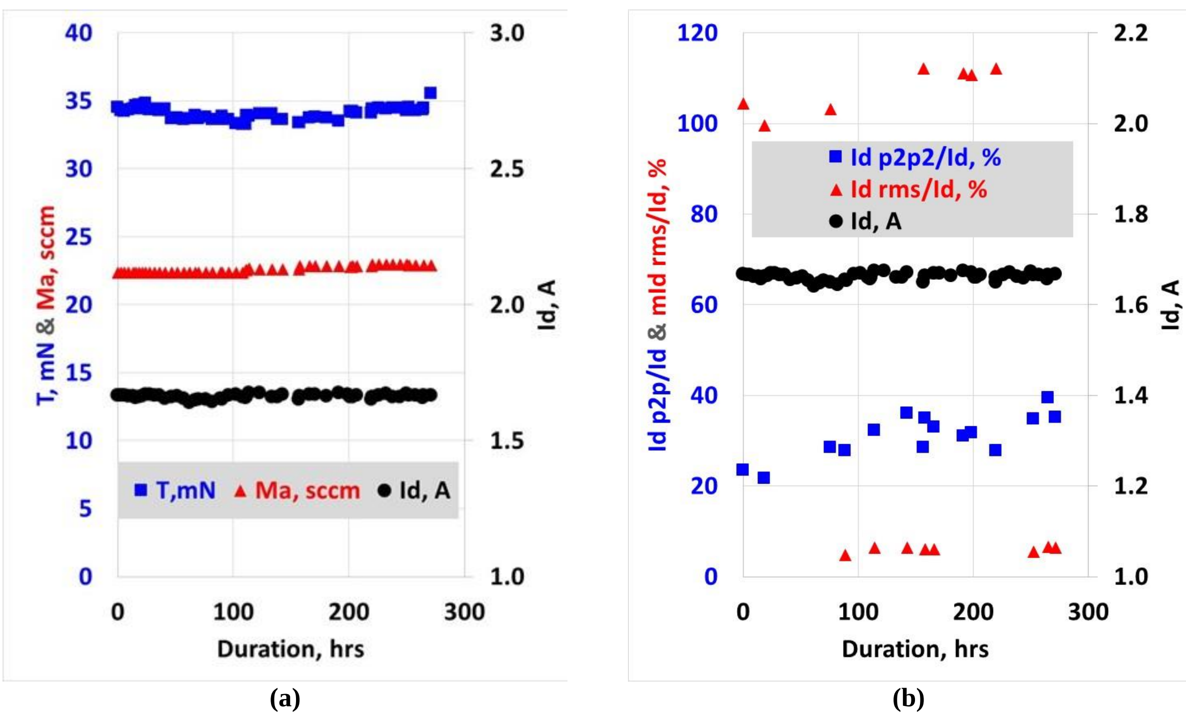

Figure 12. Variation of the H64M discharge current, thrust, anode flow rate, and discharge current ripple during the 275-hours wear test of the H64M in NASA GRC VF-8.

C. H64M Performance Characterization Post 275-hour Wear Test

After completion of the 275-hour wear test, the performance and stability characterization of the thruster were then repeated at fourteen operating conditions with the thruster in an electrically floating configuration. At each operating point, magnetic mapping was conducted across a dynamic range of 0.7 to 1.25 of nominal field setting to assess discharge stability. Figure 13 shows an example set of results for the thruster at BOL + 275 hr, with the same magnetic field settings as the data in Figure 10 and a cathode flow fraction of 7%. These test results were obtained at operational facility pressures of ~7-µTorr or lower.

After 275 hours of operations, the H64M displayed slightly lower performance compared to BOL, as typically expected during unshielded Hall-effect thruster early operation. Although, at the higher-power operating points for the 300-V and 350-V discharge voltages, where the H64M is nominally optimized to operate, the performance degradation after extended thruster operation is modest and details are provide in Table 3. This trend can be readily seen in Figure 14, which considers the 300-V discharge data from Figures 10 and 13. Table 3 presents a summary of the thruster performance pre- and post- the 275-hours wear test and shows the reduced thruster performance after extended operation.

Wear of the thruster discharge channel was measured with a chromatic, white-light non-contact benchtop profilometer. The employed profilometer is equipped with an optical pen oriented normal to the thruster exit plane with a 3-mm measuring range. Measurement of the discharge channel erosion was made by centering the thruster on the erosion measurement fixture and then performing radial profile scans at the various azimuthal locations. The measured profiles were then compared to the discharge channel BOL configuration. Preliminary analysis indicates erosion rates that are consistent with the thruster's projected propellant throughput capability of greater than 100-kg. Details on these measurement are anticipated to be presented in a future publication.

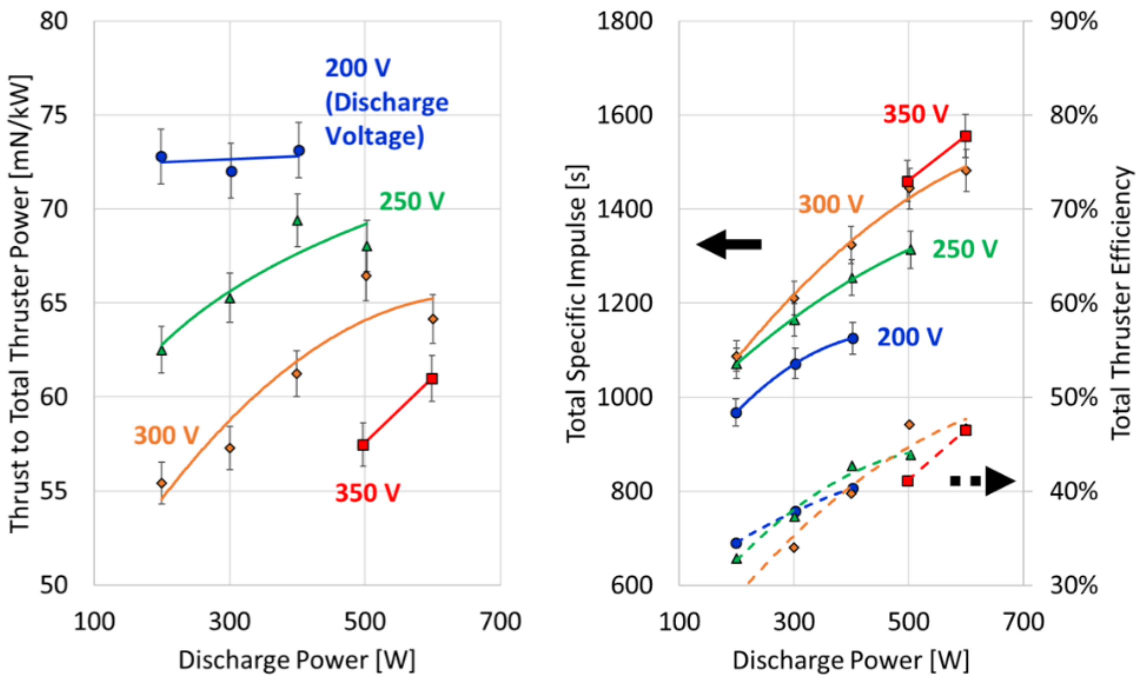

Figure 13. H64M performance at BOL + 275 hours with the same magnetic field settings as the results in Figure , 7% cathode flow fraction, and electrically floating configuration. The total thruster efficiency uncertainty bars (up to a maximum of ±5%) are not shown for clarity.

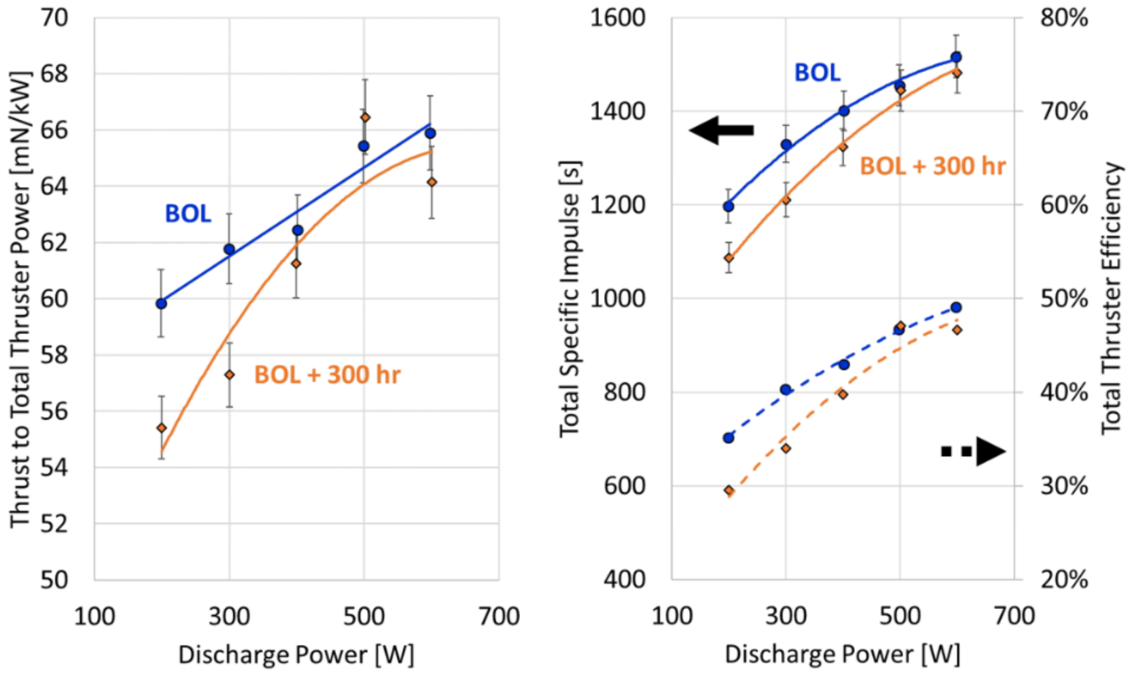

Figure 14. Comparison of H64M performance at BOL versus BOL + 275 hours for 300-V discharge voltage, identical magnetic field settings, 7% cathode flow fraction, and electrically floating configuration. The total thruster efficiency uncertainty bars (up to a maximum of ±5%) are not shown for clarity.

Table 3: Summary of 300-V and 350-V H64M BOL and BOL+275 hours thruster performance at 7% cathode fraction as presented in this paper. Maximum uncertainties are ±2% for thrust, ±3% for specific impulse, and ±5% for efficiency.

Thruster Configuration / Condition	Discharge Power [W]	Discharge Voltage [V]	Thrust [mN]	I_{sp} [sec]	η_T
H64M BOL	500	300	33	1455	47%
H64M BOL + 275 hours	500	300	34	1444	47%
H64M BOL	600	300	41	1517	49%
H64M BOL + 275 hours	600	300	40	1483	47%
H64M BOL	500	350	29	1500	42%
H64M BOL + 275 hours	500	350	29	1460	41%
H64M BOL	600	350	38	1601	48%
H64M BOL + 275 hours	600	350	37	1555	47%

D. H64M-LM Thermal Characterization Test

Thermal characterization tests of the H64M thruster were performed at four thruster operating conditions listed in Table 4. Tests were performed at the nominal magnetic field setting. The thruster was instrumented with 22 type-K thermocouples that were placed on various thruster components. Thermocouple placement was chosen to monitor the thruster component temperatures in areas of greatest thermal loading and across component interfaces. The steady-state temperature data at the various thruster operating points confirmed that the thruster's thermal design is viable since no measured thruster component temperature exceeded the designated component material's allowable temperature limit. Additionally, the thermal characterization test results supported further refinement of the thruster's thermal model, which is being used to hone the thruster's design to further its technology readiness level.

Table 4 presents the thruster's component temperatures at selected operating points. Thermal characterization test results found that as the thruster's power was ramped from 300-W to 500-W to 600-W (both at 300-V and 350-V discharge), the thruster's average component temperatures increased by 13%, 23%, and 30%, respectively. Finally, a thermal steady-state test was also performed at the thruster's operating point of 500-W (300-V discharge) at the highest thruster design magnetic field setting. That test demonstrated the thruster's inner coil assembly peak temperature did not exceed ~410ºC.

The thermal characterization test data were correlated to the results of the thermal model. The test data guided the refinement of the model thermal conductances and various surfaces emittance coefficients. The resultant correlation yields good agreement between the model predictions and the thermocouple data. For example, at the 500-W, 300-V discharge operating condition, steady-state model predictions are within 5% of the test data and show large thermal margins on component temperature limits, including the inner coil windings at the highest thruster magnetic field setting.

Table 4: H64M measured steady-state temperatures of selected thruster components at four thruster operating conditions.

Component	300W (300V) Steady State Temp [°C]	500W (300V) Steady State Temp [°C]	600W (300V) Steady State Temp [°C]	600W (350V) Steady State Temp [°C]
Outer front pole	267	300	328	349
Discharge channel exit	418	492	544	592
Outer magnet coil	234	261	282	303
Discharge channel base	329	374	411	438
Midstem/inner coil	313	356	388	408
Thruster outer core	267	299	324	343
Thruster spool mount base	164	180	191	201
Thruster back pole	304	344	375	398
Thruster mount plate	134	147	154	161

E. H64M End-Of-Life Characterization

Findings from the segments C and D were used to inform discharge channel end-of-life (EOL) configuration and geometry. A spare discharge channel was then machined to this EOL geometry and tested. The EOL accelerated wear test was performed for 100 hours. After completion of the test, no observable discharge channel erosion was detected. Figure 15a presents the thrust, anode flow rate, and discharge current variations during the 100 hours test indicating that almost no change occurred during the test duration. Figure 15b shows the variation of the discharge current ripple during the 100 hours also indicating that almost no change to the discharge current p2p or RMS occurred during this test segment.

Detailed performance characterization was performed at various thruster operating conditions; however, only results at 300 V discharge voltage operation will be reported in this paper. Figure 16a presents the thruster's performance at EOL. Results in Fig. 16a show, in general, that the thruster's performance increases as the normalized magnetic field strength is increased until a normalized field strength of ~1.1 is reached. Results in Fig. 16a also show that an efficiency of ~50% can be attained for the thruster operating at 600-W and 300-V. Finally, results in Fig 16a show that the thruster's specific impulse did not vary much as the thruster's magnetic field was varied. Figure 16b presents the discharge current ripple analysis for the thruster operating at 300-V as a function of the normalized magnetic field setting. As for the discharge current ripple, results in Fig 16b indicate that the thruster was extremely oscillatory at 300-V and 1-A; this indicates that the current density at that operating condition is too low for stable thruster operation. Increasing the discharge current to either 1.67-A or 2.0-A resulted in the thruster becoming more stable, and the level of oscillations decreased drastically as is shown in Fig 16b. Results in Fig 16b also indicate that the thruster is most stable at the nominal magnetic field setting (~1), and the oscillation levels tended to increase dramatically at magnetic field settings above the nominal value.

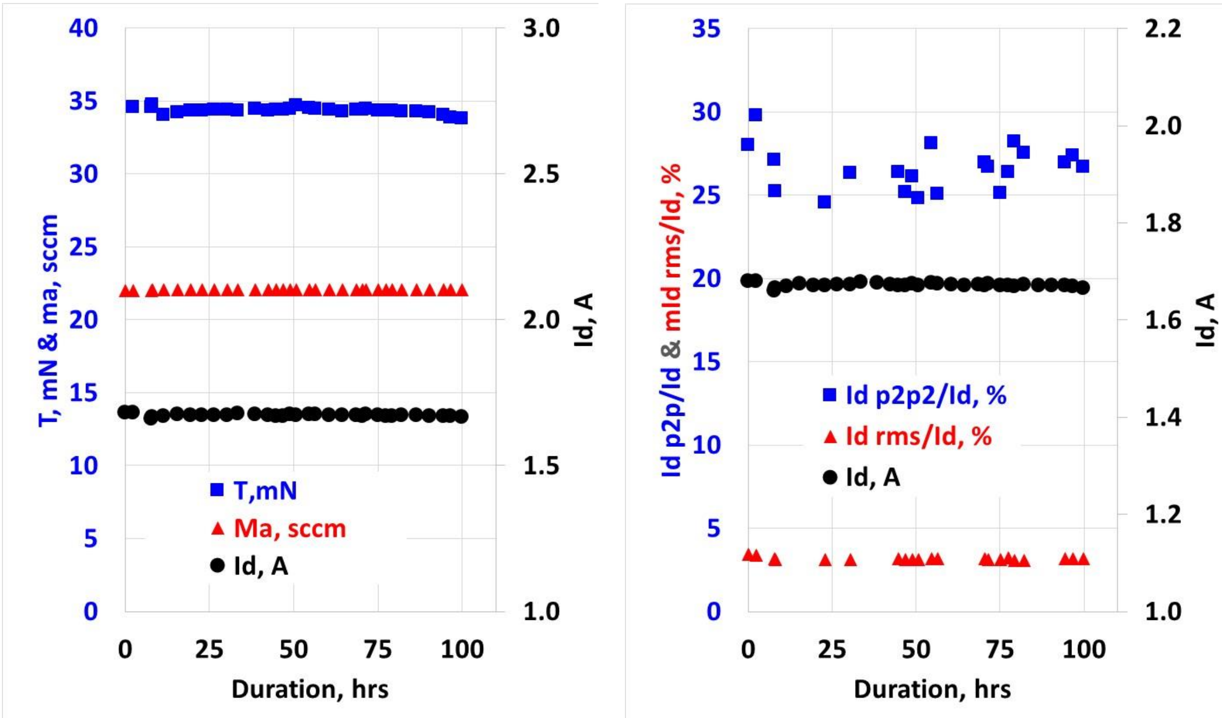

(a) (b)

Figure 15. Variation of the H64M discharge current, thrust, anode flow rate, and discharge current ripple during the 100-hours wear test of the H64M EOL discharge channel configuration in NASA GRC VF-8.

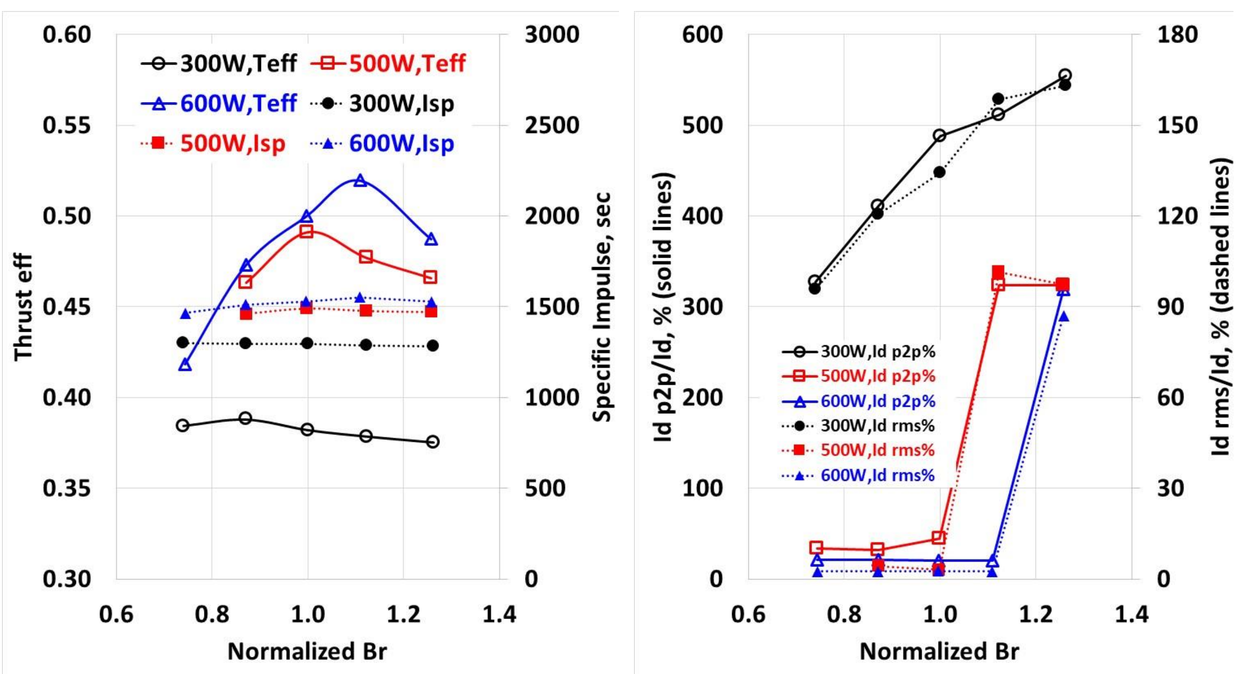

(a) (b)

Figure 16. NASA-H64M post EOL discharge channel configuration wear test performance and discharge current ripple data for 300-V discharge operation at 300-W, 500-W, and 600-W as a function of the normalized magnetic field setting.

Evaluation of different thruster electrical configurations was also performed. Tests were performed for a floating and thruster-cathode tied configuration. Results of the tests found that minimal changes in the thruster performance and discharge current ripple characteristics were observed. Table 5 summarizes the results.

Table 5: H64M-LM EOL configuration electrical configuration test summary. Test performed at discharge voltages of 300 and 350 V.

	Floating				**Cathode-Thruster Tied**			
	η	**Isp,s**	**Id p2p,%**	**Id rms,%**	**η**	**Isp,s**	**Id p2p,%**	**Id rms,%**
300W, 300V	0.37	1253	514	153	0.36	1252	504	148
500W, 300V	0.49	1481	30	3.7	0.49	1476	35	4
600W, 300V	0.51	1548	25	3	0.51	1550	26	3
600W, 350V	0.50	1624	28	3.3	0.47	1602	32	4

F. H64M-W Performance and Stability Characterization

A wider-channel version (15% wider) of the H64M thruster also underwent performance and stability characterization to assess the tradeoffs between thruster channel width and discharge channel wall strength. Having a wider discharge channel reduces inefficiencies due to wall losses and permits higher-power operation while maintaining similar plasma current density. The major drawback is that the wider the channel, the thinner and more fragile the ceramic discharge channel walls are that would be subjected to significant shock and vibration during normal spaceflight launch and operational environments. The H64M-W thruster modification was made by machining away the internal channel walls material of a spare H64M discharge channel. No modifications were made to the magnetic circuit or other thruster features.

During this test segment the thruster was operated at 300-V and 350-V discharge voltages up to 700-W discharge power. Performance and discharge current ripple data are presented in Figure 17. In Fig. 17a, thrust efficiency and specific impulse results are presented as a function of the normalized magnetic field. Results in Fig. 17a show that thrust efficiencies > 50% can be attained during thruster operation at 600-W and 700-W for discharge voltages of 300-V and 350-V. Total specific impulses above 1,500-sec are achieved for discharge power above 500-W. At a discharge power of 700-W and discharge voltage of 350-V, a specific impulse of 1,700-sec is demonstrated. Figure 16b shows that for thruster operation at 300-W and 500-W, the thruster is very oscillatory with most magnetic field settings. As the discharge power is increased to 600-W and 700-W the thruster operation becomes more stable, and there is a reasonably wide range of magnetic field operation that provides for high thruster performance at relatively low thruster discharge current ripples (with discharge current p2p and rms < 50%). Table 6 presents a summary of the thruster performance shown in Figure 16a. Table 7 summarizes the improvement in performance observed between the H64M and the H64M-W modification at 600-W discharge power. Initial test results suggest that, particularly for higher-power operations, an optimal SSEP thruster design is likely to be one with a slightly wider channel than the baseline H64M.

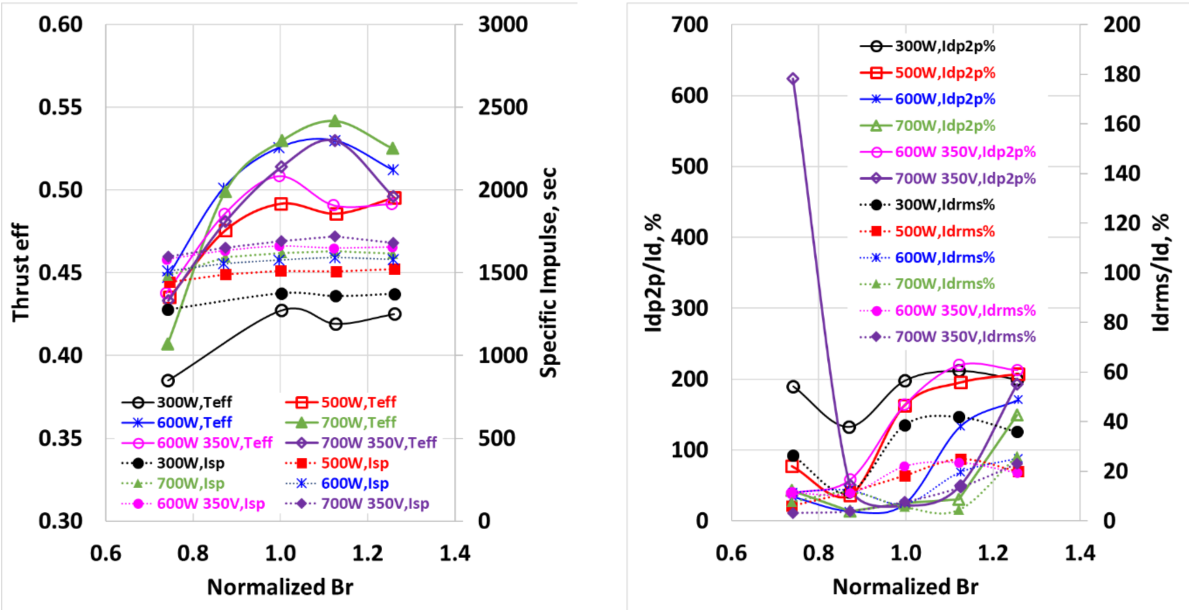

(a) (b)

Figure 17. NASA-H64M thrust efficiency and specific impulse, and discharge current ripple at beginning-of-life (BOL) with performance-optimized magnetic field strengths, 7% cathode flow fraction, and electrically floating configuration.

Table 6. Summary of 300- and 350-V H64M-W thruster performance at 7% cathode fraction as presented in this paper. Maximum uncertainties are ±2% for thrust, ±3% for specific impulse, and ±5% for efficiency.

Discharge Power [W]	Discharge Voltage [V]	Thrust [mN]	I_{sp} [sec]	η_T
600	300	42	1602	53%
700	300	48	1608	53%
600	350	38	1671	51%
700	350	44	1702	52%

Table 7. Summary of H64M-W performance improvement in comparison to H64M at BOL 600-W discharge power, 7% cathode flow fraction, and performance-optimized magnetic field strength.

Discharge Voltage [V]	*Thrust to Total Thruster Power*	*Total Specific Impulse*	*Total Thruster Efficiency*
300	1.03X	1.06X	+4%
350	1.02X	1.04X	+3%

VI. Conclusions

NASA Glenn Research Center engineering expertise, fabrication capabilities, and world-class test facilities in the field of electric propulsion facilitated the aforementioned work to be completed in one year in a single design iteration with incredible success.

The high-propellant throughput electric propulsion system advanced under the SKEP project has addressed key NASA and industry stakeholder needs, and addresses important technology development risks. The thruster work leveraged numerous prior NASA investments and produced many creative innovations to solve the unique challenges of developing a miniaturized, long-life Hall-effect electric propulsion system for small spacecraft.

Performance, stability, thermal, and wear characterization tests of the H64M thruster have demonstrated a stable and thermally-viable thruster with performance levels that exceeded the design objectives. The H64M thruster test campaign demonstrated a thruster that can achieve total thrust efficiency above 48% at specific impulse > 1,600 s at a discharge power of 600 W. Preliminary assessment from the thruster's 275-hour and EOL configuration 100-hour wear tests indicate that the thruster's discharge channel erosion rates are consistent with the thruster having a xenon throughput capability of 100 kg.

Pending continued funding, GRC aims to finish delivering an initial high total impulse capability for NASA small spacecraft science missions through collaborations with industry. The ultimate goal is to make the described thruster design available domestically to credible electric propulsion developers on a non-exclusive basis. Building on the test results from the H64M, opportunities identified for further cost and technical risk reduction, and added margin to meet collective stakeholder needs, the H71M-PM (Pathfinder Model) design was initiated in late fiscal year 2018. The H71M-PM is designed to operate at higher power than the H64M and incorporates all lessons learned for the H64M development and test campaign. GRC continues to seek opportunities to complete the HT-SSEP development, provide NASA with technology enabling lower-cost science missions, and transfer the resulting technology to domestic industry.

Acknowledgments

Numerous NASA GRC civil servants and contractors have painstakingly supported the HT-SSEP work described in this paper. The authors would like to thank Dean Petters and Tim Smith for project management; David Jacobson for technical leadership; Deb Waters for test facility management; Mike Depauw, Rich Senyitko, Nick Lalli, and Sandra Doehne for test facility leadership; Randy Clapper for design support; Matt Baird for PPU requirements development support, Jaime Scibelli for market research support, Tom Tomsik and Ryan Gilligan for feed system concept support; Bill Fabanich for thermal modeling support; Ariel Dimston for structural engineering support; Riniah Foor and the GRC fabrication shop for going above and beyond to fabricate hardware in a timely fashion; Kevin Blake and Josh Gibson for thruster assembly support; Mike Arnett, James Sadey, Tom Haag, Tom Ralys, Matt Daugherty, and Roland Gregg for test facility engineering and preparations; ZIN Technologies for engineering support, principally in PPU breadboard fabrication and testing, including Chris Sheehan, Andrew Browser, Brian Bellisario, and Charlie Druesedow; Pete Peterson, Randy Duvall, and Eric Overton for risk mitigation; and Holly Walburn for administrative support.

Reference

[1] NASA, "NASA 2018 Strategic Plan," NASA Headquarters, 2018.

[2] NASA, "Small Spacecraft Technology - State of the Art," NASA/TP–2018-220027.

[3] McGuire, M. L., Hack, K. J., Manzella, D. H. and Herman, D. A., "Concept designs for NASA's Solar Electric Propulsion Technology Demonstration Mission," 50th AIAA/ASME/SAE/ASEE Joint Propulsion Conference, Cleveland, OH, AIAA-2014-3717.

[4] https://standards.nasa.gov/standard/gsfc/gsfc-std-7000.

[5] Kamhawi, H., Mackey, J., Frieman, J., Huang, W., Gray, T., Haag, T., and Mikellides, I., "HERMeS Thruster Magnetic FieldnTopology Optimization Study: Performance, Stability, and Wear Results," IEPC-2019-902, 36th International Electric Propulsion Conference, Vienna, Austria, Sept. 2019.

[6]Baranov, V., Nazarenko, Y., and Petrosov, V., "Azimuthal Non-Uniformities in Accelerators with Closed Electron Drift," IEPC-2001-018.

[7]Reid, B. M., "The Influence of Neutral Flow Rate in the Operation of Hall Thrusters," Ph.D. dissertation, University of Michigan, 2009.

[8] Huang, W., and Yim, J., "Propellant Distributor for a Thruster". USA Patent 10,273,944, 30 April 2019.
[9] Patterson, M. J., Foster, J. E., Haag, T. W., Pinero, L., and Soulas, G. C., "Ion propulsion development activities at the NASA Glenn Research Center," 39th AIAA/ASME/SAE/ASEE Joint Propulsion Conference, AIAA-2003-4709.
[10] Domonkos, M. T., Gallimore, A. D., and Patterson, M. J., "Parametric Investigation of Orifice Aspect-Ratio on Low Current Hollow Cathode Power Consumption," 34th AIAA/ASME/SAE/ASEE Joint Propulsion Conference and Exhibit, Cleveland, OH, AIAA 1998-3345.
[11] Williamson, W. S., Dulgeroff, C. R., Williams, R. L., and Bayless, J. R., "8-cm Engineering Model Thruster Technology: A Review of Recent Developments," 14th International Electric Propulsion Conference, Princeton, New Jersey, AIAA-1979-2103.
[12] Patterson, M. J., Domonkos, M. T., Carpenter, C., and Kovaleski, S. D., "Recent Development Activities in Hollow Cathode," 27th International Electric Propulsion Conference, Pasadena, California, IEPC-2001-270.
[13] Kohl, W. H., *Handbook of Materials and Techniques for Vacuum Devices*, New York: Reinhold, 1967, p. 494.
[14] Ham, R. K., Williams, J. D., Hall, S. J., Benavides, G. F., and Verhey, T. R., "Characterization of propellant flow and bias required to initiate an arc discharge in a heaterless hollow cathode," 55th AIAA/SAE/ASEE Joint Propulsion Conference, Indianapolis, IN, 2019.
[15] Myers, J. L., Kamhawi, H., Yim, J. T., and Clayman, L. K., "Hall Thruster Thermal Modeling and Test Data Correlation," 52nd AIAA/SAE/ASEE Joint Propulsion Conference, Salt Lake City, UT, AIAA-2016-4535.
[16] Haag, T. W., "Thrust Stand for High-Power Electric Propulsion Devices," Review of Scientific Instruments, Vol. 62, No. 5, 1991.
[17] Mackey, J. A., Haag, T. W., Kamhawi, H., Hall, S. J., and Peterson, P. Y., "Uncertainty in Inverted Pendulum Thrust Measurements," NASA/TM-2018-219952.
[18] Kamhawi, H., Haag, T. W., Huang, W., Herman, D. A., Williams, G. J., Peterson, P. Y., Hofer, R. R., and Mikellides, I. "Performance, Stability, and Pressure Effects Characterization Tests of NASA's 12.5-kW Hall Effect Rocket with Magnetic Shielding (HERMeS) Thruster," AIAA-2016-4826, 52nd AIAA/SAE/ASEE Joint Propulsion Conference. Salt Lake City, UT, 2016.
[19] Peterson, P. Y., Kamhawi, H., Huang, W., Williams, G., Gilland, J., Yim, J., Hofer, R. R., and Herman, D. "NASA's HERMeS Hall Thruster Electrical Configuration Characterization," AIAA-2016-5027 *52nd AIAA/ASME/SAE/ASEE Joint Propulsion Conference*. AIAA, Salt Lake City, UT, 2016.
[20] Szabo, J., Pote, B., Tedarke, R., Paintal, S., Byrne, L., Hruby, V., Kamhawi, H., and Smith, T., "High Throughput 600 Watt Hall Effect Thruster for Space Exploration," AIAA-2016-4830, 52nd AIAA/SAE/ASEE Joint Propulsion Conference. Salt Lake City, UT, 2016.
[21] Conversano, R. W., Goebel, D. M., Mikellides, I. G., Hofer, R. R., and Wirz, R. E., "Performance Analysis of a Low-Power Magnetically Shielded Hall Thruster: Computational Modeling," *AIAA J. Propuls. Power*, vol. 33, no. 4, pp. 992–1001 (2017).
[22] Conversano, R. W., Lobbia, R. B., Tilley, K. C., Goebel, D. M., Reilly, S., Mikellides, I. G., and Hofer, R. R., "Development and Initial Performance Testing of a Low-Power Magnetically Shielded Hall Thruster with an Internally-Mounted Hollow Cathode," IEPC-2017-64, *35th International Electric Propulsion Conference*, Atlanta, GA, Oct. 2017.
[23] Garner, C., Brophy, J., Polk, J, "A 5.730-Hr Cyclic Test of the SPT-100," AIAA-95-2667.